Available online at www.sciencedirect.com
ScienceDirect
Journal of Power Sources 161 (2006) 587–593
JOURNAL OF POWER SOURCES
www.elsevier.com/locate/jpowsour

Tin–graphite materials prepared by reduction of $SnCl_4$ in organic medium: Synthesis, characterization and electrochemical lithiation

L. Balan [a], R. Schneider [b], P. Willmann [c], D. Billaud [a,*]

[a] *LCSM, UMR CNRS 7555, UHP Nancy I, BP 239, 54506 Vandoeuvre-les-Nancy Cedex, France*
[b] *SOR, UMR CNRS 7565, UHP Nancy I, BP 239, 54506 Vandoeuvre-les-Nancy Cedex, France*
[c] *CNES, 18 Avenue E. Belin, 31055 Toulouse Cedex, France*

Received 11 July 2005; received in revised form 11 January 2006; accepted 4 April 2006
Available online 24 May 2006

Abstract

Tin–graphite materials were prepared by chemical reduction of $SnCl_4$ by *t*-BuONa-activated NaH. TEM imaging showed that the crude material is composed of an amorphous organic matrix containing tin present either as nanosized particles deposited on the graphite surface or as free aggregates. Subsequent washings with ethanol and water allow removal of side products as well as most part of the organic matrix. Electrochemical insertion of lithium occurred in graphite and in tin. The initial reversible massic capacity of 630 mAh g^{-1} decayed to a stable value of 415 mAh g^{-1} after 12 cycles. This capacity value was lower than the expected maximum one of 650 mAh g^{-1} corresponding to a Sn/12C molar composition and assuming the formation of LiC_6 and $Li_{22}Sn_5$. Even if this massic capacity is not much improved by comparison with that of graphite, it must be pointed out that the volume capacity of this graphite/Sn material is much larger (2137 mAh cm^{-3}) than that corresponding to graphite (837 mAh cm^{-3}). It was hypothesized that the part of tin bound to graphite could be responsible for the stable reversible capacity. To the contrary, graphite unsupported tin aggregates would contribute to the observed gradual decline in the storage capacity. Therefore, the improvement in cycleability, compared to that of massive metals, could be attributed both to the nanoscale dimension of the metal particles and to interactions between graphite and metal the nature of which remaining to be precised.

Keywords: Lithium-ion battery; Graphite; Tin; Anodic material; Chemical reduction

1. Introduction

Graphitic carbons are the most widely used among the commercial negative electrodes of Li-ion batteries [1]. Historically they were preferred to lithium and lithium alloys for the development of lithium-ion cells since they display the best compromise in terms of large specific charge and reversible cycling behavior [2].

The maximum theoretical specific charge of graphite which corresponds to the formation of the stage I LiC_6 graphite intercalation compound is equal to 372 mAh g^{-1}. Such a capacity is obtained at a low voltage, typically lower than 0.3 V versus Li^+/Li. The low volume variation accompanying Li intercalation/deintercalation (up to 10%) allows the electrode to retain its mechanical integrity upon cycling. However, the continuous demand to further increase both specific energy and long life cycling has stimulated the research for new electrode materials [3–5]. Some metals able to alloy lithium were prepared as substitution material to graphite. However, during alloying, they were submitted to large volume variations which cause pulverization of the electrode. As a result, fast capacity fading is observed [6].

It was demonstrated that these drawbacks can be partly overcome by reducing the metal particle size and by using multiphase systems or alloys [6–10]. An alternative way for improving the electrode properties consists in associating lithium storage metals of high capacity to carbonaceous materials [11–15].

We recently showed that metal chlorides ($SbCl_5$, $BiCl_3$ and $SnCl_2$) could be reduced by KC_8, a strong reducing graphite intercalation compound. The resulting Sb, Bi and Sn-based systems are able to insert lithium reversibly [16,17]. Their electrochemical performance as anodic material of Li-ion batteries was discussed in terms of metal particle size crystallinity of the lithium storage element and of their ability to be bound with graphite [16–18].

* Corresponding author. Tel.: +33 3 83 68 46 22; fax: +33 3 83 68 46 23.
E-mail address: billaud@lcsm.uhp-nancy.fr (D. Billaud).

0378-7753/$ – see front matter © 2006 Elsevier B.V. All rights reserved.
doi:10.1016/j.jpowsour.2006.04.065

Bi–graphite and Sb–graphite systems were also elaborated by reduction in the presence of graphite of $BiCl_3$ and $SbCl_5$ with activated NaH in organic media [14,15,18]. In these materials, nanosized metal particles are supported on graphite and are embedded in an alkoxide matrix. An improved and stable reversible capacity is obtained with the Sb-based material.

This article reports the synthesis of Sn–graphite materials obtained by reduction of $SnCl_4$ by *t*-BuONa-activated NaH and the evaluation of their suitability as negative electrode for Li-ion batteries.

2. Experimental

Anhydrous tin(IV) chloride (Aldrich) was used as received. Tetrahydrofuran (THF) was distilled from sodium benzophenone adduct and stored over sodium wires. Sodium hydride (Fluka, 65% in mineral oil) was used after two washings with THF. *tert*-Butyl alcohol (*t*-BuOH) was distillated over Na. The reduction was handled under standard airless techniques in a nitrogen atmosphere as described in our previous paper [19].

In a Schlenk tube, *t*-BuONa-activated NaH in THF and graphite (UF4 Carbone Lorraine) were mixed for 5 min. $SnCl_4$ is then injected dropwise to the reaction medium. The Schlenk content was further stirred at 65 °C for 2 h. The solution was then rotary evaporated under air to remove volatile organics, which led to a black powder of *t*-BuONa stabilized Sn(0) particles and graphite. Afterwards, all handlings were performed under argon or nitrogen atmosphere. The products of reaction were submitted to X-ray diffraction (XRD) analysis using the Mo Kα radiation of an automated powder diffractometer (Rotoflex Ru-200B, Rigaku generator and CPS 120 INEL detector transmission assembly). Transmission electron microscopy (TEM) studies (image mode and selected area electron diffraction (SAED)) were performed with a Philips CM20 microscope operating at 200 kV. Elemental analysis was carried out by energy dispersive X-ray spectrometry (EDXS) with an EDAX spectrometer. Samples were previously dispersed in THF by sonication. A drop of the sonicated suspension was deposited on a carbon observation grid and then introduced into the microscope column.

Electrochemical insertion of lithium was performed in half cells. A lithium ribbon was used both as reference and auxiliary electrodes. The electrolyte was $LiClO_4$ (1.5 mol kg^{-1})–ethylene carbonate (EC) solution. A 1-methyl-2-pyrrolidinone slurry of the Sn/graphite material (95 wt.%) and polyvinylidene fluoride (PVDF) binder (5 wt.%) was used to coat a copper current collector. Excess of solvent was evaporated under primary vacuum. Electrochemical studies were monitored by a Mac Pile II apparatus operating in galvanostatic and voltammetry modes. In the galvanostatic mode (charge and discharge processes), the output voltage was recorded for a specific current cell of 20 μA mg^{-1} applied for 6 min followed by a 10 s relaxation period. In voltammetry studies, the current was monitored when the voltage was scanned by steps of 2.4 mV applied for 2 min between 0 and 2.5 V versus Li^+/Li.

3. Results and discussion

3.1. Synthesis of the (graphite/tin)-based material

We have recently reported a new organometallic synthesis of size-controlled tin(0) nanoparticles which used *t*-BuONa-activated NaH as the reducing agent of $SnCl_4$ [19]. This method has been extended to the reduction of $SnCl_4$ in the presence of graphite. The chemical reaction for the synthesis of the

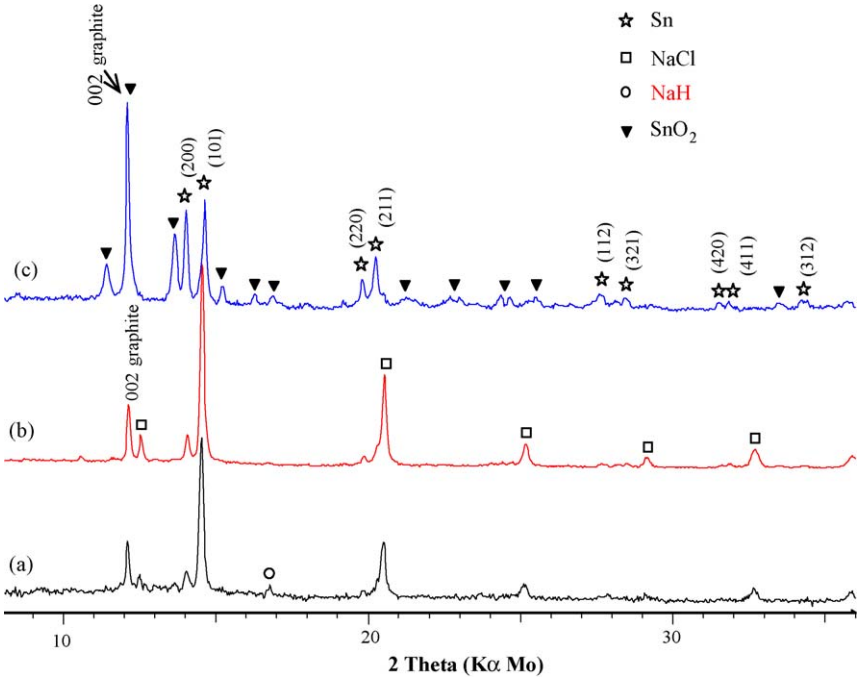

Fig. 1. XRD patterns of the Sn/graphite-based system: (a) as-synthesized, (b) after washing with EtOH and (c) after washing with H_2O.

(graphite/tin)-based material can be formulated as:

$$SnCl_4 + 4NaH/2t\text{-BuONa} + \text{graphite} \xrightarrow[65^\circ C]{THF} \text{graphite/Sn(0)}/2t\text{-BuONa} + 2H_2 + 4NaCl$$

In our experiment, the atomic C/Sn ratio is equal to 12. This technique to synthesize Sn(0) nanoparticles takes advantage of the weak coordinating properties of *t*-BuONa which acts as a stabilizer and avoids aggregation of the metal particles formed during the reduction.

3.2. X-ray diffraction characterization

Fig. 1 presents the XRD patterns of the crude material resulting from the reduction of $SnCl_4$ by *t*-BuONa-activated NaH in the presence of graphite (Fig. 1a), after washing with ethanol (Fig. 1b) and after washing with ethanol and water (Fig. 1c). Reduction of $SnCl_4$ was effective since reflections of both Sn(0) and NaCl are present on the crude material obtained after synthesis (Fig. 1a). As shown in Fig. 1b, the excess of NaH used for the reduction step was removed by washing with ethanol (Fig. 1b) while NaCl was eliminated by further washing with water (Fig. 1c). Extra reflections of orthorhombic SnO_2 are also present in Fig. 1c indicating that a part of tin(0) is oxidized during washing with water [20]. The 0 0 2 graphite reflection pointed at 336 pm indicates that graphite is not modified during the reduction. The coherence length along the graphite *c*-axis, L_c, was estimated from the value of the full width at one-half height of the 0 0 2 reflection according to the Scherrer formula ($L_c = 0.9\lambda/\beta \cos\theta$) [21]. Such a value L_c is equal to 29 nm. Tin(0) was also present as evidenced by the reflections of the tetragonal structure of tin.

In Fig. 1a and b, the average size of tin cristallites is about 5 nm using the Scherrer formula. After washing with water (Fig. 1c), aggregation and coalescence of Sn(0) particles occur leading to the obtention of tin crystallites of about 36 nm in size. During subsequent washings, not only NaCl is removed but also most of the organic matrix. In fact, diffuse reflectance infrared Fourier transform studies (DRIFT) carried out on materials obtained by $BiCl_3$ reduction with activated NaH showed a strong attenuation of bands characteristic of the organic matrix, composed in majority of *t*-BuONa. It is obvious that the washings allow to eliminate most of the matrix [28]. These data can be reasonably extrapolated to the systems obtained by reduction of other chlorides with activated NaH.

3.3. TEM characterization

TEM observation of the crude material obtained after reduction of $SnCl_4$ by *t*-BuONa-activated NaH was also carried out. Fig. 2a presents the bright field image showing the presence of

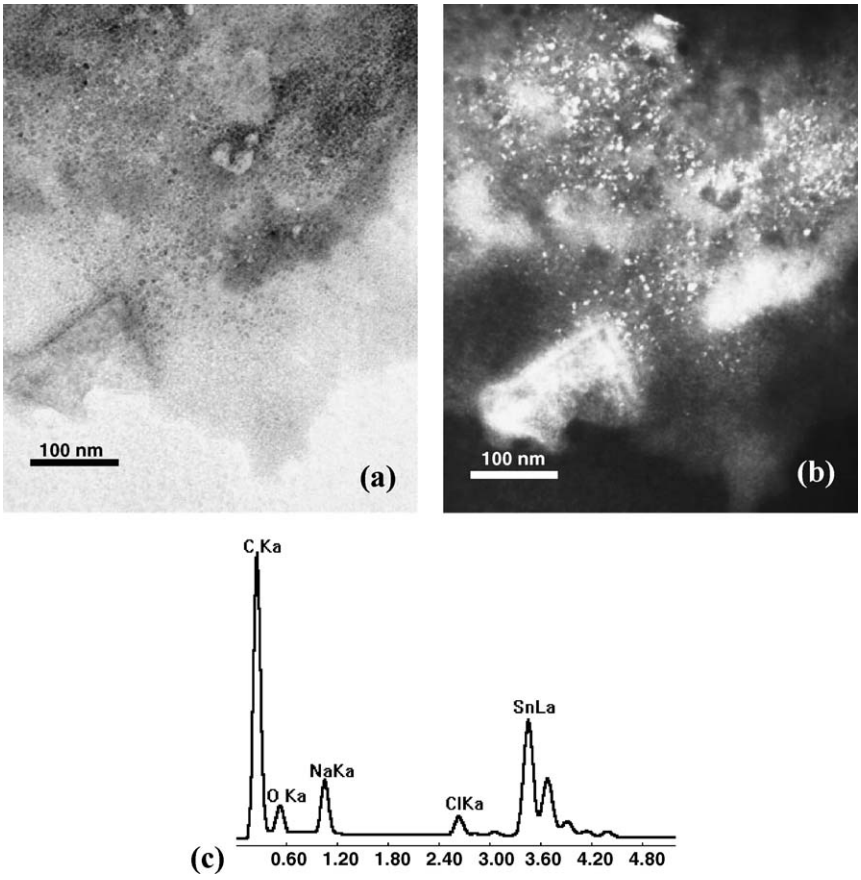

Fig. 2. TEM studies of the as-prepared graphite/Sn material: (a) bright field micrograph, (b) dark field micrograph and (c) EDXS analysis.

nanosized particles with a diameter of 4.2 ± 0.1 nm embedded in the *t*-BuONa organic matrix. The related dark field micrography shown in Fig. 2b gives evidence for the crystalline structure of tin particles. It must be pointed out that tin particles are not only dispersed on the graphite surface but are also present as independent nodules. The corresponding EDXS spectrum (Fig. 2c) shows that the elements expected in the products obtained after reduction are present. The excess of Na compared to that expected in NaCl is related to Na contained in the amorphous organic matrix. Washing the crude material with ethanol results in the elimination of the excess NaH used during the synthesis. The bright field micrograph of the obtained material (Fig. 3) shows that tin is present as aggregates of various sizes. The average diameter of these aggregates is about 24 nm.

Fig. 4a shows the bright field micrograph of the material obtained after washing with ethanol and water. Tin particles appear more agglomerated. Some polygonal nanoprisms displaying spherical, triangular and hexagonal outlines can be observed on the TEM micrograph. The average size of tin aggregates is equal to 34 nm, value in good accordance with the XRD data. The related SAED pattern (Fig. 4b) displays in the [2 2 0] zone axis diffraction spots characteristic of the tin tetragonal structure (space group *I*41/*amd*).

Comparison of the micrographs presented in Figs. 2a, 3 and 4a gives evidence for the elimination of the amorphous organic matrix which is no more observable after ethanol and water washings.

3.4. Electrochemical study

Fig. 5 shows selected current versus potential curves obtained for the (Sn/graphite)-based system at a rate of 2.5 mV per 2 min, after ethanol and water washings. In the first reduction profile, several peaks are present. The negative current observed at the highest potentials can be related to the irreversible reduction

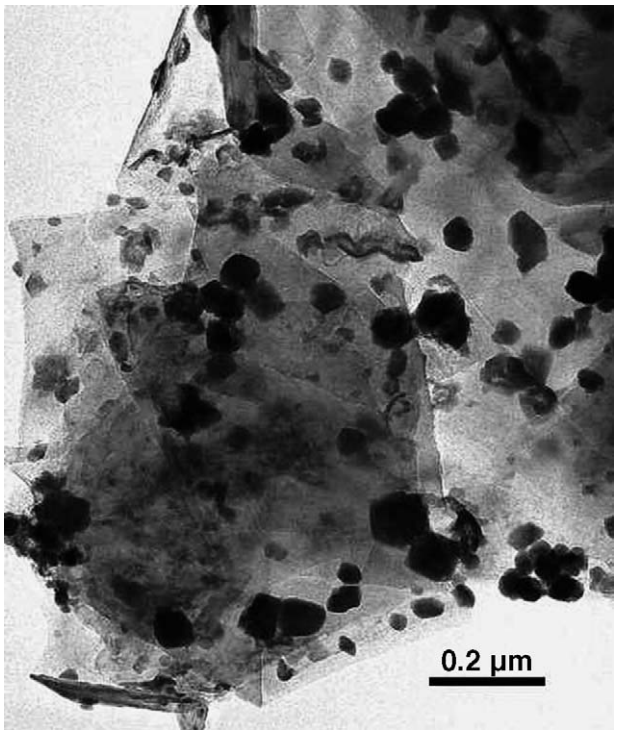

Fig. 3. TEM micrograph of the graphite/Sn material after washing with EtOH.

of tin oxide SnO_2 formed during the washing with water and handlings, according to the following reaction:

$$SnO_2 + 2Li^+ + 2e^- \rightarrow SnO + Li_2O$$

$$SnO + 2Li^+ + 2e^- \rightarrow Sn + Li_2O$$

In the literature, SnO_2 and SnO reductions are completed at 1.88 and 1.58 V, respectively. One must point out that oxidized tin particles are embedded in an organic matrix that increases

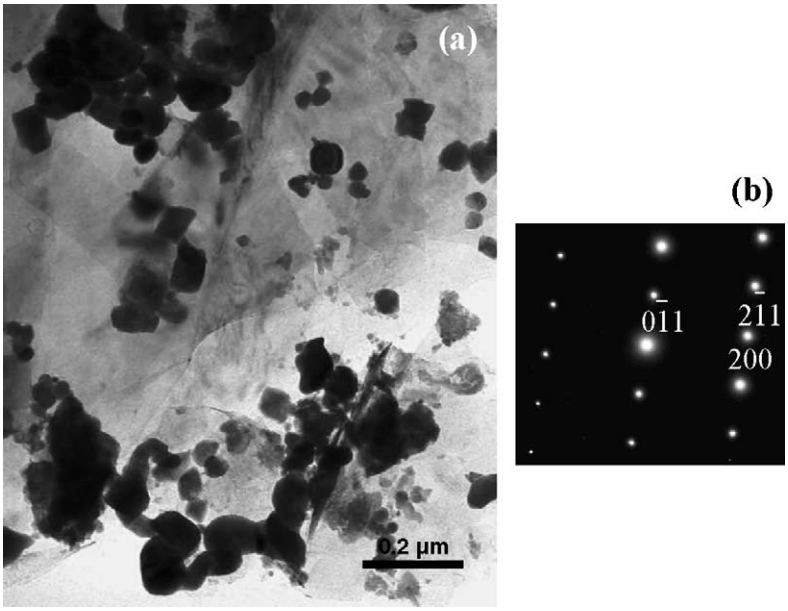

Fig. 4. (a) TEM micrograph of the graphite/Sn material after washing with EtOH and H_2O and (b) related SAED pattern.

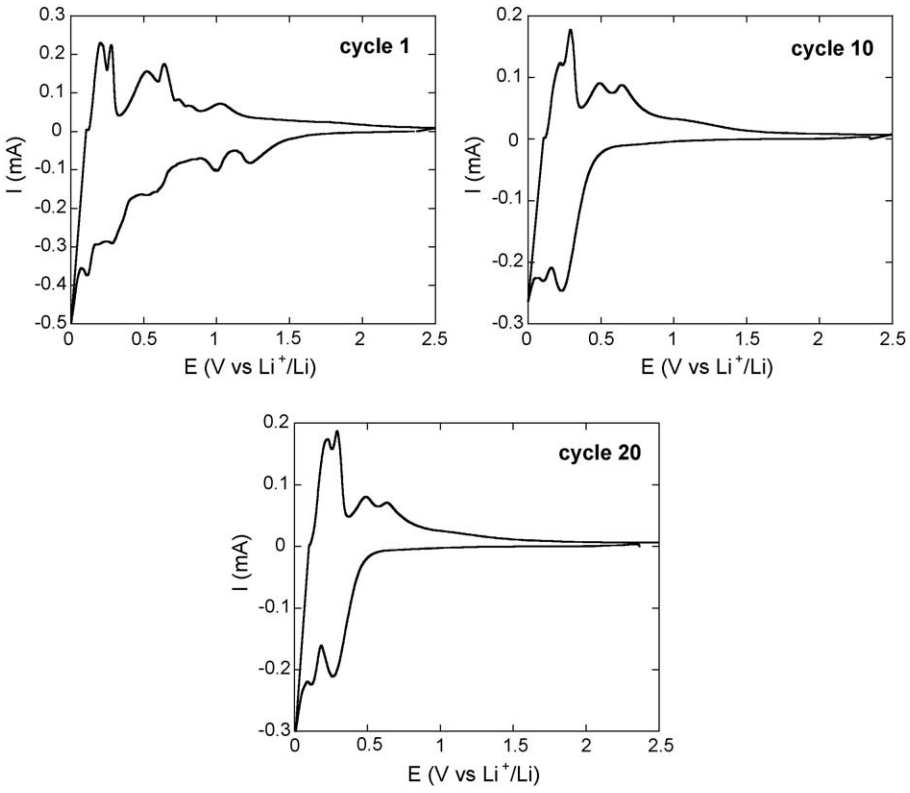

Fig. 5. Selected current vs. potential curves of the graphite/Sn-based system obtained after washing with EtOH and H_2O.

the electrical resistance of the electrode with consequently a displacement of the reduction potentials towards lower potential values [8,22]. Below 0.9 V, the negative current can first be related to the formation of the solid electrolyte interphase (SEI) on graphite and Sn surfaces [6,23], then to the formation of Li_xSn alloys [22,24–26] and to lithium intercalation into graphite [27]. According to the literature and to our previous results, Li_xSn alloys (Li_2Sn_5, LiSn, Li_7Sn_3, Li_5Sn_2, $Li_{13}Sn_5$ and $Li_{22}Sn_5$) are formed in the 0.76–0.38 V potential region. In the deinsertion process, peaks present below 0.2 V are related to the reversible lithium deintercalation out of graphite. Peaks appearing at higher potentials correspond to lithium dealloying.

Some differences in the intensity profiles are evidenced between the first cyclic voltammogram and the following ones. Tin oxides reduction results in the obtention of amorphous tin and in the irreversible formation of the insulating Li_2O which affects the resistance of the electrode and also the kinetics of lithium insertion. As already observed in previous papers related to lithium insertion into Sn and carbon–Sn-based materials, the number of peaks related to lithium alloying and dealloying is depending on the crystallinity and on the thickness of Sn particles [29,30]. For instance, according to Sumiya et al. [29], a 30 nm thick crystalline Sn film evaporated on a graphitized mesophase carbon fiber, displays a cyclic voltammogram presenting in one hand only a sharp peak besides a very low intense one in the reduction process, and, in an other hand, three sharp peaks in the oxidation process. Both anodic and cathodic peak intensities decay upon cycling. After amorphization of tin obtained by tin oxide reduction, the cyclic voltammogram has changed: with a 30 nm thick amorphous Sn film-based materials, the cyclic voltammogram displays the same number of peaks which however have broadened; with a Sn nm thick amorphous Sn film-based material, the major broad peak present in the reduction process is associated to two broad peaks in the oxidation wave. The intensity of these peaks becomes stable after a few charge/discharge cycle. Therefore, with amorphous tin, the peaks related to Li_xSn formation broaden and collapse. Moreover, the kinetics of Li insertion and extraction into these alloys are probably depending on their composition. As a result, the number of peaks observed in the reduction and in the oxidation processes can differ. The cyclic voltammograms of our graphite/Sn materials are characteristic of amorphous compounds. The five peaks related to Li_xSn dealloying broaden upon cycling and collapse to give only two broad and intense peaks associated, at the highest potentials, to a very broad and low intensity peak. In the alloying process, only one broad and intense peak corresponding to the superimposition of several ones is present. These data are similar to those obtained with the graphite/Sn systems synthesized by reduction of $SnCl_2$ with KC_8 in THF medium [17]. In this case, the amorphous organic matrix is not present due to the synthesis process and the material is only composed of Sn particles either deposited on graphite or in the form of free aggregates. However, the shapes and the number of peaks present in the reduction and oxidation are the same than that is observed with the graphite/Sn materials described in this manuscript. That it an evidence that our washing procedure leads to the elimination of the organic matrix and that the properties of the graphite/Sn systems elaborated by two differ-

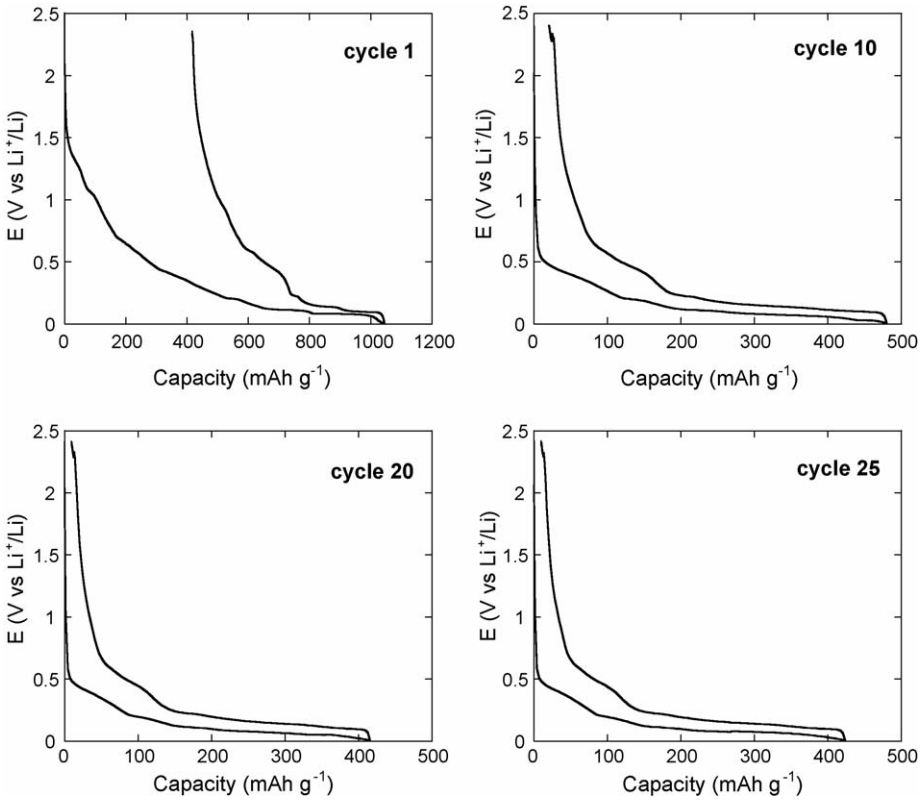

Fig. 6. Selected charge and discharge curves of graphite/Sn composite washed with ethanol and water.

ent synthesis processes are similar. During repetitive cycling, the intensity of the peaks corresponding to lithium dealloying decreases first and then reaches a stable value. The decrease of the reversible tin capacity is likely related to the presence of tin aggregates not bound to graphite [17]. These tin aggregates are submitted to large volume variations generated by lithium insertion and extraction. These variations result in the pulverization of the aggregates in smaller size particles which are electrically disconnected, leading to the decay of the reversible capacity.

Fig. 6 displays selected charge/discharge curves recorded for a specific current of 20 μA mg^{-1} applied in the 0–2.4 V potential window. The pseudo potential plateaus are related to the peaks present in the corresponding voltammograms. Assuming the formation of the highest lithium content alloy, $Li_{22}Sn_5$, and the formation of LiC_6, the expected theoretical maximum specific charge of the 12C/Sn system is equal to 653 mAh g^{-1}. In this total capacity, 204 and 449 mAh g^{-1} correspond to graphite and tin, respectively. The irreversible capacity observed during the first charge/discharge cycle is close to 400 mAh g^{-1}. This value can be mainly related to tin oxides reduction and to the SEI formation on tin and graphite. A significant contribution of the organic matrix is not expected since it was mostly removed by ethanol and water washings. In the following cycles, the irreversible capacity decreases rapidly with the cycle number, likely in connection with the formation of the SEI on the tin particles generated by the aggregates pulverization occurring during lithium insertion. This fact is supported by a careful examination of the profile of the reduction curves showing a decrease of the curve length in the 0.5–0.2 V range. The reversible experimental capacity close to 630 mAh g^{-1} in the first cycle decreases up to a stable value of 415 mAh g^{-1} (12th cycle) as presented in Fig. 7. Such a decrease of the reversible capacity during the first cycles could be due to lithium insertion into free tin particles and aggregates not bound to graphite and which behave as massive tin [16,17]. The presence of graphite in the reaction medium during reduction of tin chloride by activated NaH results in a stabilization of the reversible capacity. On the contrary, when graphite is mixed with the material obtained after reduction of tin chlorides with activated NaH, the initial reversible capacity is lower and decays rapidly upon cycling. In such a case of a physical mixture, there is no direct contact between graphite and tin particles which are covered with an oxide layer [32]. The direct contact and likely bond between

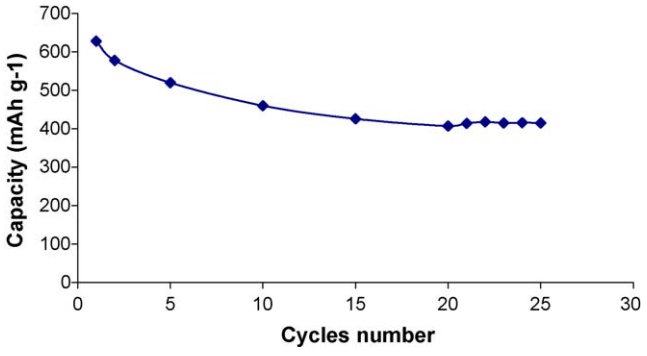

Fig. 7. Evolution of the reversible capacity upon cycling of the graphite/Sn composite.

tin and graphite is needed to obtain a stable reversible capacity by a mechanism which remains to be precised. That means, by hypothesizing that the pratical capacity of graphite is contant at 192 mAh g^{-1}, that the fraction of tin which cycles reversibly goes down from 97.5 to 50%. About one-half of tin content is therefore expected to be disconnected from graphite. The other half part of tin is probably bound to graphite by chemical (covalent) bonds. Preliminary ^{119}Sn and ^{121}Sb Mössbauer spectroscopic studies carried out on Sn/graphite and Sb/graphite materials would indicate that the Mössbauer parameters (isomershift and quadrupole splitting) of Sn and Sb, in the free state and involved in our Sn/graphite-based materials are different [31].

4. Conclusion

In this study, a new tin-based graphite material has been prepared as candidate for the negative electrode of lithium-ion batteries. The synthesis of such system was performed by reduction of $SnCl_4$ using *t*-BuONa-activated NaH in the presence of graphite. XRD and TEM measurements show that tin is crystallized in the expected tetragonal structure and that the size of Sn(0) particles is dependent on the washing treatment. Nanometer-sized Sn(0) particles produced after synthesis slowly coalesce into larger aggregates possessing an average size of 34 nm after washing with ethanol and water.

Electrochemical lithium insertion in the washed material gives evidence for lithium intercalation into graphite and for lithium–tin alloys formation. A stable reversible capacity of 415 mAh g^{-1} is found. Such a value is lower than the maximum theoretical capacity of 650 mAh g^{-1} assuming the formation of LiC_6 and $Li_{22}Sn_5$. It could be hypothesized that the reversible capacity would be related to the fraction of tin bound to graphite. Free tin particles or aggregates are supposed to behave like massive elemental tin during lithium insertion. This leads to a substantial change in the specific volume generating cracks and pulverization of the material with consequently a loss of the electrical contact and a capacity fade upon cycling. Extra studies are needed in order to decrease the fraction of tin not bound to graphite and the size of tin(0) particles. That supposes to increase the contact area between metal and graphite by decreasing the metal particle size and/or increasing the (graphene(*ab*)plane/(thickness along *c*-axis)) ratio of the graphite particles. The determination of free and graphite-bound tin can be evaluated by Mössbauer and electron energy loss spectroscopies. Such characterization are currently in progress to support our hypothesis that a stable and high reversible capacity of our metal–graphite systems could be obtained only with nanosized metal particles bound to graphite. Finally, it must be pointed out that even if the massic capacity (415 mAh g^{-1}) is not much improved with respect to natural graphite (372 mAh g^{-1}) the volumic capacity of our materials, close to 2137 mAh cm^{-3}, is by far larger than that of LiC_6 (837 mAh cm^{-3}). Such an improvement of the volumic capacity is expected for satisfying the strong demand of production of miniaturized handy electronic appliances.

Acknowledgements

Dr. J. Ghanbaja is hereby gratefully acknowledged for skilful TEM characterization and valuable discussions. The Centre National d'Etudes Spatiales (CNES) is warmly thanked for financial support.

References

[1] T. Nagaura, K. Tazawa, Prog. Batteries Solar Cells 9 (1990) 209–217.
[2] M. Winter, J.O. Besenhard, M.E. Spahr, P. Novak, Adv. Mater. 10 (10) (1998) 725–763.
[3] J. Yang, Y. Takeda, N. Imanishi, J.Y. Xie, O. Yamamoto, Solid State Ionics 96 (2000) 277–281.
[4] J.O. Besenhard, J. Yang, M. Winter, J. Power Sources 68 (1) (1997) 87–90.
[5] O. Crosnier, T. Brousse, X. Devaux, P. Fragnaud, D.M. Schleich, J. Power Sources 94 (2001) 169–174.
[6] M. Winter, J.O. Besenhard, Electrochim. Acta 45 (1–2) (1999) 31–50.
[7] T. Brousse, R. Retoux, U. Herterich, D.M. Schleich, J. Electrochem. Soc. 145 (1) (1998) 1–4.
[8] I.A. Courtney, J.R. Dahn, J. Electrochem. Soc. 144 (1997) 2045–2049.
[9] Y. Itoda, T. Kubota, A. Matsufuji, Y. Maekawa, T. Miyasaka, Science 276 (1997) 1395.
[10] P.E. Lippens, J. Olivier-Fourcade, J.C. Jumas, Hyperfine Interact. 126 (2000) 137–141.
[11] J.Y. Lee, R. Zhang, Z. Liu, J. Power Sources 90 (2000) 70–75.
[12] J. Santos-Pena, T. Brousse, D.M. Schleich, Solid State Ionics 135 (2000) 87–93.
[13] J. Read, D. Foster, J. Wolfenstine, W. Behl, J. Power Sources 96 (2001) 277–281.
[14] A. Dailly, P. Willmann, D. Billaud, Electrochim. Acta 48 (2002) 271–278.
[15] A. Dailly, J. Ghanbaja, P. Willmann, D. Billaud, J. Power Sources 136 (2004) 281–284.
[16] A. Dailly, L. Balan, J. Ghanbaja, P. Willmann, D. Billaud, Carbon 43 (2005) 1001–1008.
[17] L. Balan, J. Ghanbaja, P. Willmann, D. Billaud, Carbon 43 (2005) 2311–2316.
[18] A. Dailly, J. Ghanbaja, P. Willmann, D. Billaud, Electrochim. Acta 48 (2003) 977–984.
[19] L. Balan, R. Schneider, D. Billaud, J. Ghanbaja, Nanotechnology 16 (2005) 1153–1158.
[20] E. Mueller, Acta Crystallogr. Sec. B: Struct. Sci. 40 (1984) 359.
[21] H.P. Klug, L.E. Alexander, X-ray Diffraction Procedures for Polycrystalline and Amorphous Materials, second ed., Wiley/Interscience, New York, 1974, pp. 687–692.
[22] W. Liu, X. Huang, Z. Wang, H. Li, L. Chen, J. Electrochem. Soc. 145 (1998) 59–61.
[23] R.A. Huggins, Solid State Ionics 113–115 (1998) 57–67.
[24] A. Naji, J. Ghanbaja, B. Humbert, P. Willmann, D. Billaud, J. Power Sources 63 (1996) 33–39.
[25] J. Wang, I.D. Raistrick, R.A. Huggins, J. Electrochem. Soc. 133 (1986) 457–460.
[26] I.A. Courtney, J.R. Dahn, J. Electrochem. Soc. 144 (1997) 2943–2949.
[27] D. Billaud, F.X. Henry, P. Willmann, Mater. Res. Bull. 28 (1993) 477–483.
[28] L. Balan, Ph.D. Thesis, University of Nancy I, 2005.
[29] K. Sumiya, J. Suzuki, R. Takasu, K. Sekine, T. Takamura, J. Electroanal. Chem. 462 (1999) 150–156.
[30] J. Li, H. Li, Z. Wang, X. Huang, L. Chen, J. Power Sources 81–82 (1999) 346–351.
[31] L. Balan, A. Dailly, R. Schneider, D. Billaud, J.C. Jumas, J. Olivier-Fourcade, P. Willmann, Hyperfine Interactions, in press.
[32] D. Billaud, L. Balan, R. Schneider, P. Willmann, Carbon, in press.